CHAPTER V

WAVELENGTH INFLUENCE ON MASS SPECTRA IN IR-MALDI

Given the wide range of materials and laser parameters utilized in MALDI, it is quite likely that there is no generic model able to describe the phenomena associated with material removal. As noted in previous chapters, one of the remarkable features of MALDI is that it is applicable for a wide range of material systems and irradiation conditions. In Chapter 3, we saw that similar MALDI spectra could result from a wide range of laser conditions. Just as these irradiation conditions necessarily created vastly different initial electronically or vibrationally excited states, so to the initial physical states depend on the combination of irradiation and material parameters, and thus determine the ablation pathways.

In this chapter the progress made towards better understanding the mechanism of material removal in IR-MALDI is presented, primarily by examining the energy absorption into specific vibrational modes. In Chapter 4 we found that the density of vibrational excitation, and thus the character of the ablation plume, had a significant effect on the ion species observed due to the efficiency of the sample disintegration (Section 4.3.1). Here we describe a more complicated relationship, where the efficiency of ion production is not directly related to the solid-state absorption coefficient. The effect of the excitation wavelength is also examined for laser damage to single crystals of matrix materials and the 'quality' of the mass spectra. These results are compared with calculations of the heat transfer and acoustic wave propagation to define the operative ablation mechanism. To establish a proper context for these results, Section 5.1 reviews important parameters infrared laser ablation processes, while Section 5.2 describes previous studies on the infrared wavelength dependence of MALDI spectra.

5.1. Infrared laser ablation processes

Material removal is a complex process that depends critically on the irradiation parameters, including the laser wavelength, fluence and pulse duration, as well as the optical and thermomechanical properties of the material, such as the wavelength dependent absorption coefficient, thermal diffusivity, defect concentration and tensile strength. Additionally, the

optical and thermal properties may be temperature- and pressure-dependent, but these relationships known for many of the materials used in MALDI. In rough order of increasing energy, possible mechanisms of material removal include vaporization, spallation, explosive boiling, and phase explosion. Excellent discussions of these processes have been reported from both experimental and computational perspectives [2-7], and a brief summary of the processes likely germane to MALDI are discussed below.

Irradiation with ultraviolet lasers causes electronic excitation, which can then relax through a variety of radiative or non-radiative processes. Electron-phonon scattering results in vibrational motion, often accompanied by the generation of defects that destabilize the lattice through Coulomb forces; on a time scale of hundreds of picoseconds, these localized vibrational modes dissipate their energy into the harmonic phonon bath that constitutes the heat bath of the matrix, leading to bond-breaking and ejection of atoms, ions, molecules and even clusters [8]. Infrared irradiation directly initiates vibrational motion, and the various ablation pathways depend critically on the various time scales and length scales in which that energy deposition is accomplished. If the deposited energy can relax away from the irradiated volume before critical temperatures and pressures are reached, simple vaporization and melting result. However, if the energy is absorbed before the thermal diffusion from the volume is realized, a condition known as thermal confinement occurs. This can lead to overheating of the material beyond the boiling point, turning normal surface evaporation into explosive vaporization, or phase explosion, at higher fluences [5,6]. It has been predicted, based on thermodynamic considerations, that phase explosion results in simultaneous decomposition of the ejected plume into a two-phase sytem of gas-phase molecules and liquid droplets [5,6]. In a one-dimensional picture, justified by the large aspect ratio between laser spot size diameter and penetration depth into the sample, the thermal transport time, τ_{th}, can be approximated by

$$\tau_{th} = \frac{\rho c_p}{4\lambda_{th}} \delta^2 \tag{5.1}$$

where δ is the laser penetration depth, ρ is the density of the material, c_p is the specific heat, and λ_{th} is the thermal conductivity. There have been a number of studies, however, noting that violent material ejection can occur at energies much less than those needed for explosive boiling. Another non-equilibrium condition leading to massive material ejection occurs when the energy

Table 5.1 Thermal and acoustic transport times for select modes of $NaNO_3$ and succinic acid

	ρ (kg/m^3)	c_p (J/kg·K)	λ_{th} (W/m·K)	δ (μm)	τ_{th} (ns)	τ_{ac} (ns)
$NaNO_3$ 7.2 μm	2260	1082	565	0.07	530	0.023
$NaNO_3$ 3.6 μm	2260	1082	565	8	$7x10^6$	2.6
Succinic acid, 2.9 μm	1570	1300	0.2	40[1]	$4x10^6$	13
Succinic acid, 3.4μm	1570	1300	0.2	20[1]	$1x10^6$	7

[1] Penetration depth values from [1].

is delivered into a volume on a time scale shorter than the energy can be dissipated by acoustic relaxation, τ_{ac}, a condition known as stress confinement. This can result in strong compressive thermoelastic pressure, which when interacting with the free surface of the irradiated sample can lead to tensile stresses which exceed the strength of the material. This can result in cavitation, the formation of microcracks, and eventually removal of fractured platelets from the surface. The relevant time constant for acoustic transport is approximated by

$$\tau_{ac} = \delta \nu_s^{-1} \tag{5.2}$$

where ν_s is the speed of sound in the material. Assuming a value of 3000 m/s for ν_s, τ_{ac} and τ_{th} are calculated for several absorption modes in Table 5.2. The thermal transport times are longer, and significantly longer for 3 cases, than the laser pulses used, suggesting that thermal confinement is operative. However, τ_{ac} is on the order of the 100 ns pulse train used in our studies, suggesting that spallation is likely to be a minor contributor to material removal. When considering ablation pathways, one must consider the laser repetition rate, for if the system has only partially relaxed prior to the subsequent pulses, then the 'baseline' temperature of the system will gradually increase until a critical threshold is reached and the system cools by material ejection [9].

The few research groups practicing IR-MALDI have primarily utilized fixed frequency lasers, such as the Er:YAG (2.94 μm), Er:YSGG (2.79μm) and CO_2 (9.25, 9.6 and 10.6 μm), although more recently tunable lasers like the free-electron laser (2-10 μm) and optical parametric oscillators (2-4 μm). These lasers can deposit energy into the OH, CH, CO and NH

absorption bands, making almost any organic compound a potential matrix material, provide that other requirements of a MALDI matrix, chemical compatibility with the analyte and the ability to assist in ion formation, are met.

5.2. Previous studies of the wavelength dependence in IR-MALDI

The above discussion of the importance of the density of excitation in determining ablation mechanisms offers a compelling explanation to the results from Chapter 4 showing increased cation formation efficiency at a strongly absorbing mode. A good correlation of the reciprocal of the threshold fluence with the matrix absorbance has been found in UV-MALDI [10-12]. However, the assumption that the degree of resonant vibrational excitation is the primary determinant for a successful IR-MALDI experiment appears somewhat presumptuous in light of several wavelength studies of IR-MALDI matrices. Several reports have observed that when targeting the OH band near 3 μm, the wavelength requiring the least energy and also providing the best spectra is blue-shifted with respect to the absorption peak, in some cases to a wavelength where insignificant bulk absorption occurs [1,13-18]. Explanations for this phenomenon include modified absorption profiles by weakly hydrogen-bound OH and NH groups, shifted absorption profiles under ablation conditions, strong contributions from surface or interstitial molecules, and absorption by residual solvent. Weakened hydrogen bonds could be caused by thermal or mechanical disruption of the sample by the leading edge of a laser pulse, shifting the absorption profile, so that the end of the pulse - or subsequent pulses – are able to more efficiently reduce the ablated material to molecular species or promote charge transfer. The OH stretching vibration of free carboxylic acids occurs at $2.81 - 2.86$ μm and the free alcohol OH stretching vibrations range from $2.74 - 2.79$ μm [19], near the observed energy minimum for compounds with these functional groups. Unfortunately, gas-phase spectra of these compounds, have not yet been reported. These discrepancies have been shown to not be related to absorption by the substrate [1]. Little data exists of the absorption profile of matrix compounds under the high temperature and pressure conditions realized in laser ablation, but one study suggests that the absorption of liquid water shifts several hundred nanometers to shorter wavelengths under intense laser irradiation [20], in keeping with the magnitude of the observed blue-shift. A careful study of the possible role of residual water, however, strongly suggests that

either water incorporated during crystallization or waters of hydration are unable to explain the threshold fluence profile [13]. Surface species also have absorption maxima shifted to higher frequencies, and threshold energies are lower for samples with greater surface area [17]. Ions have also been found preferentially at the leading edge of ablation plumes [21,22], although this is not necessarily related to their spatial formation. Given the volume of material removed during a typical IR ablation event (10^4 μm), it may be surprising that such a large contribution comes from surface species, but since the ion:neutral ratio is believed to be less than 10^{-4}:1 [23,24], this possibility should not be discounted. Finally, the broad absorption bands of water extend to shorter wavelengths than MALDI matrix compounds, and since water is known to function as a matrix material [25,26], even at small concentrations [27], recent observations of solvent inclusions in crystals [28] suggest that these solvents could play a role in sample absorption. Menzel says that succinic does not incorporate water into the crystal 36-38.

Reports of wavelength studies near the CH stretching mode near 3.4 μm show both a direct correlation between the absorption cross section and threshold energy, *i.e.*, less energy is required at the peak of the absorption mode [13,14] and a less clear relationship [1]. Near the C=O vibration, a smaller but significant blue-shift is found in the few cases studied [1,17]. Several absorption modes of glycerol near 10 μm have been studied with the available frequencies from CO_2 lasers, and while the three wavelengths tested produced acceptable mass spectra, there was poor correlation between the absorption cross section and mass spectra performance [29]. A number of these studies have found that when comparing two different absorption bands for the same matrix, there is no correlation between the absorbance values and threshold energies [1,14,29].

Several of these wavelength studies have noted that the 'quality' of the spectra, *i.e.* the reduction of low mass peaks, improved signal-to-noise ratio and mass resolution are also wavelength dependent, and in most cases the more favorable spectra are generated at wavelengths where the energy threshold is the lowest. (Generally, in UV-MALDI, the best mass spectrometric performance was obtained at wavelengths near the absorption maximum, though a direct comparison with this observation should be treated with caution given the significant differences in absorption cross-sections.) Despite the obvious practical advantages and potential implications for understanding mechanisms, little commentary has been provided on this rather remarkable feature for IR-MALDI. A similar improvement in spectra quality has described as

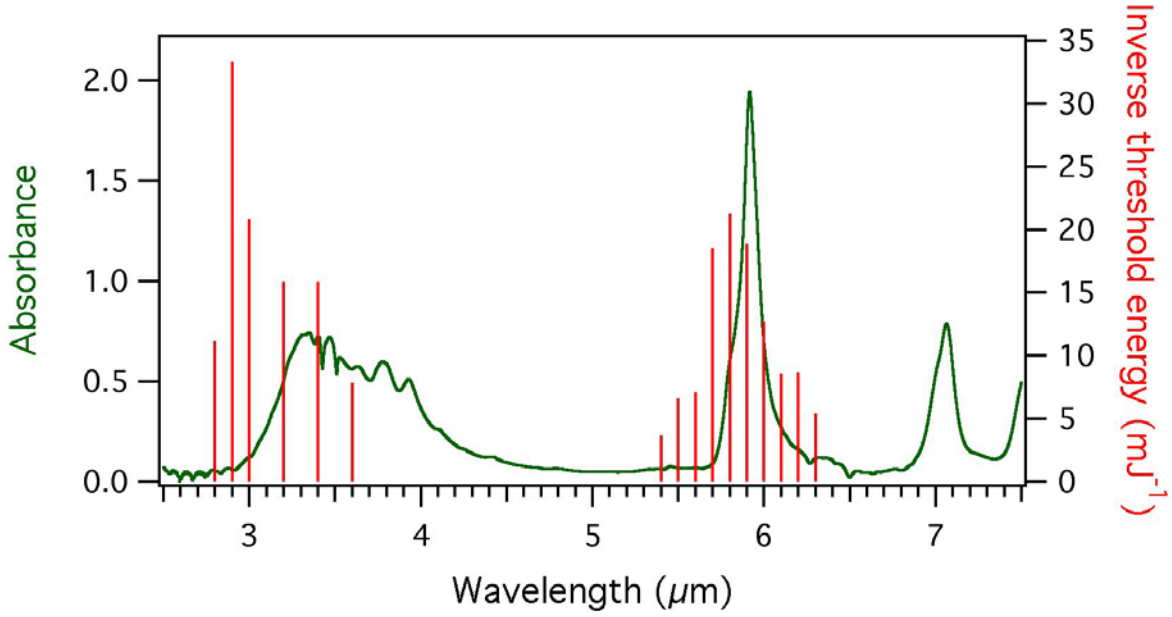

Figure 5.1. The inverse energy thresholds (red sticks) for the appearance of neurotensin from a succinic acid matrix plotted against the absorbance spectra of succinic acid (green trace). The most efficient wavelength, *i.e.* the one requiring the lowest energy, in the 3 µm range is found to be 2.9 µm, which is shofted with respect to the OH absorption curve, which peaks near 3.3 µm. Like wise, near the CO band at 5.9 µm, the lowest energy threshold is at 5.8 µm, again to the short wavelength side.

the matrix suppression effect, mentioned in Section 4.2.2, where it appears that the analyte's higher proton affinity allows it to abstract all free charge in the dense plume, provided there is a sufficient concentration of analyte [30,31]. However, as the same sample can yield both matrix-free spectra and matrix-dominating spectra at different wavelengths, such a comparison seems speculative. One explanation is that irradiation at different wavelengths results in different plume species, and at the 'more favorable' wavelength equilibrium conditions exist and the favorable abstraction of protons by the analyte is allowed to go to completion. At the 'less efficient' wavelength, the collisions are kinetically limited, resulting in a mixture of matrix and analyte ion species. The difference between the kinetic and equilibrium conditions has previously been examined by adjusting the laser fluence, assuming that the higher fluences result in denser plumes, and thus equilibrium conditions, in accordance with the presented data [32]. A simple test of this phenomenon would be to determine if the mass dependence and analyte concentration ratios observed in UV-MALDI are also observed in IR-MALDI.

5.3. Energy thresholds as a function of wavelength

Figure 5.1 shows the relationship between the minimum energy necessary to see ions (energy threshold) and the absorption of succinic acid. The absorbance spectrum was acquired in attenuated total reflection (ATR) mode, (Section 2.4) which may not accurately reflect the absorption characteristics of the surface layers of the sample. The bands investigated include the overlapping broad OH stretching mode centered at 3.33 μm and the CH stretching mode at 3.43 μm, as well as the C=O stretching mode at 5.91 μm. The analyte detected here was neurotensin in succinic acid at a $1{:}10^4$ molar ratio. The sticks represent the inverse of the threshold energy required to see analyte ions, and so should qualitatively scale with the absorption spectrum if bulk absorption is the determining parameter in ion generation. However, in agreement with earlier studies, that the wavelength requiring the least energy is shifted to shorter wavelengths near both the 3 and 6 μm regions, while modest agreement is seen near 3.5 μm. In agreement with earlier results, the increase of the threshold energy on the longer wavelength side is more gradual than on the short wavelength side, where the analyte ion signal quickly disappears for wavelengths below 2.8 μm. Analyte signal is obtained on the higher wavelength side at wavelengths up to 3.6 μm. Unfortunately, experiments at wavelengths in the 3.6-4.2 μm range, where there is still an appreciable absorption coefficient, were not attempted in this study. Other studies of succinic acid report threshold energies up to 3.6 μm but neglect to comment on the performance at longer wavelengths.

Deuterated succinic acid was used to attempt and differentiate the role a specific absorption mode might contribute to the generation of ions. In addition to the unsubstituted acid, designated as succinic-d_0, the d_4 analogue compound, shown in Figure 5.2, was studied. Energy thresholds for wavelengths in the 7-8 μm region and are displayed in Figure 5.3. Band assignment were made based on values found in the literature [33]. The succinic-d_0 sample showed the following modes in the 7-8 μm region: at 7.05 μm, weak CH_2 scissoring bands are covered by strong intermolecular OH--H hydrogen bonds, and a C-O stretching mode (7.09 μm) is coupled to an OH bending vibration at 7.65 μm, denoted by the asterisks. The succinic-d_4 sample also shows the weakened intermolecular OH--H bands at 7.05 μm and the coupled C-O stretching mode (7.09 μm) and OH bending vibration (shifted to7.72 μm). However, the succinic-d_4 was prepared in deuterated methanol and experienced significant HD substitution on the carboxyl hydrogens as evidenced by bands in the CH_2 (3.4 μm) and CD_2 (4.7 μm) stretching

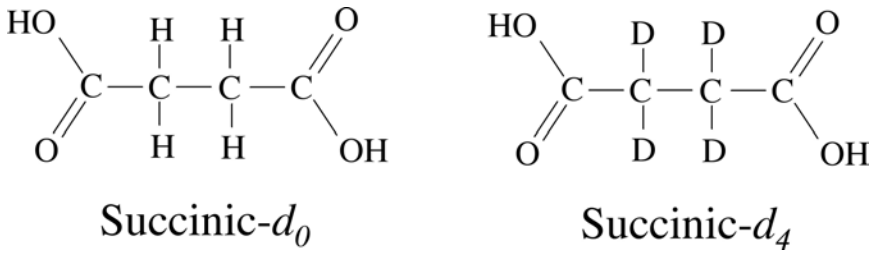

Figure 5.2. Structures of succinic-d_0 and succinic-d_4 used in the deuterated studies.

regions (not shown). This resulted in the weakening of the intermolecular OH--H and the C-O stretching bands near 7.05 μm and a new band at 7.36 μm due to C-O coupling with the OD bending vibration.

The comparison here does not provide clear evidence of a mode specific response, but suggests that the absorption profile alone is a poor indicator for determining ion formation. It should be noted that the bandwidth of the FEL in this wavelength range was about ±0.4 of the central frequency. The band near 7.0 μm, which contains several overlapping bands, does not

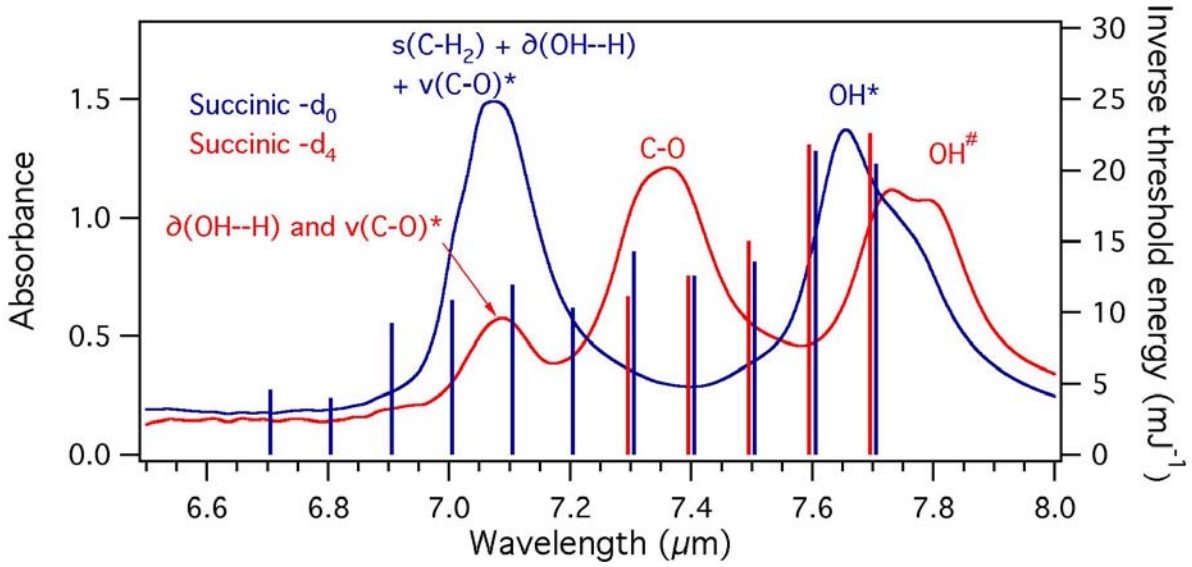

Figure 5.3. Inverse energy thresholds plotted against the FTIR ATR absorbance spectra for succinic-d_o (blue trace) and succinic-d_4 acids (red trace). The inverse threshold values are represented as blue (succinic-d_o) and red (succinic-d_4) sticks from the x-axis (right axis) and represent the energy thresholds for seeing angiotensin II analyte signal according to the protocol defined in the text. The band assignments listed here are described further in the text. No signal was seen for irradiation at 6.6 μm at the available laser energy for succinic-d_0 scan, while wavelengths beyond 7.7 μm were not tested for either compound. The shortest wavelength attempted for succinc-d_4 was 7.3 μm.

show a shift in the threshold energy, contrary to the C=O and O-H stretching modes but in agreement with the CH stretch. For succinic-d_0, the data shows a surprising decrease in energy threshold as the absorption decreases near 7.4 μm, and then a decrease as the absorption from the OH band contributes. While it is known that the absorption of free OH shift to the blue near the 3 μm region, it is not known if such a shift is observed for this coupled mode. In the 7.3-7.5 μm region, it appears that for succinic-d_4, the increased absorption due to the C-O band (coupled to the OD mode) does not cause a significant decrease in threshold fluence. To the author's knowledge, the only studies of the role of the substrate have shown no contribution at a specific wavelength [1,13].

5.4. Summary

The fundamental parameter in these wavelength studies, except for the obvious appearance or non-appearance of analyte ions, was the threshold energy. There appears to be only a weak correlation between the density of excitation in the material and the direct generation of ions. This represents a contrast to the results of Chapter 3, but that study required the lower energies associated with cation formation as opposed to likely mechanism of cation formation seen here. Earlier studies of the wavelength dependence showed a energy threshold blue shift when groups directly involved in intermolecular binding were probed, such as OH and C=O, but not for aliphatic or aromatic CH modes. In the deuterated succinic acid studies we see an even more confusing behavior. Improved understanding of the operative mechanisms present at different wavelengths will require measurements of different experimental parameters, such as the photoacoustic studies currently underway [29], analysis of laser damage craters, measurements of the density and size distribution of the plume at several temporal stages, and measurements of the initial ion velocities. Ion velocities measured at 2.94 μm were slightly higher than those measured from ultraviolet experiments [25,34], but both wavelength regimes suggest a jet-like expansion of material into the gas-phase. However, as the mechanisms of ablation are known to depend on absorption cross-section, as mentioned in Chapter 4, as well as pulse durations, as discussed above, irradiation at wavelengths with different cross sections by

lasers with varied pulse durations may help pinpoint the important parameter set for efficient ion generation.

BIBLIOGRAPHY

[1] R. Cramer, R. F. Haglund, and F. Hillenkamp, International Journal of Mass Spectrometry **169/170**, 51 (1997).

[2] S. Georgiou and A. Koubenakis, Chemical Reviews **103** (2), 349 (2003).

[3] L. V. Zhigilei, E. Leveugle, B. J. Garrison, Y. G. Yingling, and M. I. Zeifman, Chemical Reviews **103** (2), 321 (2003).

[4] R. F. Haglund, in *Laser ablation and desorption*, edited by R. F. Haglund (Academic Press, New York, 1998).

[5] A. Miotello and R. Kelly, Applied Physics a-Materials Science & Processing **69**, S67 (1999).

[6] R. Kelly and A. Miotello, Physical Review E **60** (3), 2616 (1999).

[7] A. Miotello and R. Kelly, Nuclear Instruments & Methods in Physics Research Section B- Beam Interactions with Materials and Atoms **122** (3), 458 (1997).

[8] N. Itoh and A. M. Stoneham, *Materials processing by electronic excitation*. (Oxford University Press, Oxford, 2001).

[9] E. G. Gamaly, A. V. Rode, and B. Luther-Davies, Journal of Applied Physics **85** (8), 4213 (1999).

[10] V. Horneffer, K. Dreisewerd, H. C. Ludemann et al., International Journal of Mass Spectrometry **187**, 859 (1999).

[11] X. J. Chen, J. A. Carroll, and R. C. Beavis, Journal of the American Society for Mass Spectrometry **9** (9), 885 (1998).

[12] D. A. Allwood, R. W. Dreyfus, I. K. Perera, and P. E. Dyer, Applied Surface Science **110**, 154 (1997).

[13] Christoph Menzel, Klaus Dreisewerd, Stefan Berkenkamp, and Franz Hillenkamp, International Journal of Mass Spectrometry **207** (1-2), 73 (2001).

[14] Jay D. Sheffer and Kermit K. Murray, Rapid Communications in Mass Spectrometry **12** (22), 1685 (1998).

[15] K. L. Caldwell and K. K. Murray, Applied Surface Science **129**, 242 (1998).

[16] K. L. Caldwell, D. R. McGarity, and K. K. Murray, Journal of Mass Spectrometry **32** (12), 1374 (1997).

[17] Wayne P. Hess, Hee K. Park, Oguz Yavas, and R. F. Haglund Jr., Applied Surface Science **127-129**, 235 (1998).

[18] R. Cramer, F. Hillenkamp, and R. F. Haglund, Journal of the American Society for Mass Spectrometry **7** (12), 1187 (1996).

[19] L. J. Bellamy, *The infrared spectra of complex molecules*, 3rd ed. (Chapman and Hall, London, 1975).

[20] K. L. Vodopyanov, Journal of Chemical Physics **94** (8), 5389 (1991).

[21] A. A. Puretzky and D. B. Geohegan, Chemical Physics Letters **286** (5-6), 425 (1998).

[22] K. R. Chen, T. C. King, J. H. Hes et al., Physical Review B **60** (11), 8373 (1999).

[23] C. D. Mowry and M. V. Johnston, Rapid Communications in Mass Spectrometry **7** (7), 569 (1993).

[24] A. A. Puretzky, D. B. Geohegan, G. B. Hurst, M. V. Buchanan, and B. S. Luk'yanchuk, Physical Review Letters **83** (2), 444 (1999).

[25] Stefan Berkenkamp, Christoph Menzel, Franz Hillenkamp, and Klaus Dreisewerd, Journal of the American Society for Mass Spectrometry **13** (3), 209 (2002).

[26] M. L. Baltz-Knorr, K. E. Schriver, and Jr. Haglund, R. F., Applied Surface Science **197-198**, 11 (2002).

[27] S. Berkenkamp, M. Karas, and F. Hillenkamp, Proceedings of the National Academy of Sciences of the United States of America **93** (14), 7003 (1996).

[28] Verena Horneffer, Rudolf Reichelt, and Kerstin Strupat, International Journal of Mass Spectrometry **226** (1), 117 (2003).

[29] Klaus Dreisewerd, Stefan Berkenkamp, Arne Leisner, Andreas Rohlfing, and Christoph Menzel, International Journal of Mass Spectrometry **226** (1), 189 (2003).

[30] Richard Knochenmuss, Volker Karbach, Ursula Wiesli, Kathrin Breuker, and Renato Zenobi, Rapid Communications in Mass Spectrometry **12** (9), 529 (1998).

[31] R. Knochenmuss, F. Dubois, M. J. Dale, and R. Zenobi, Rapid Communications in Mass Spectrometry **10** (8), 871 (1996).

[32] K. Breuker, R. Knochenmuss, J. Zhang, A. Stortelder, and R. Zenobi, International Journal of Mass Spectrometry **226** (1), 211 (2003).

[33] M. Suzuki and Shimanou.T, Journal of Molecular Spectroscopy **28** (3), 394 (1968).

[34] D. R. Ermer, M. Baltz-Knorr, and R. F. Haglund, Journal of Mass Spectrometry **36** (5), 538 (2001).